Astronomy & Astrophysics manuscript no. CEMPs18
January 14, 2016
©ESO 2016

arXiv:1601.03385v1 [astro-ph.SR] 13 Jan 2016

The role of binaries in the enrichment of the early Galactic halo.

III. Carbon-enhanced metal-poor stars – CEMP-*s* stars

T.T. Hansen[1], J. Andersen[2,3], B. Nordström[2,3], T. C. Beers[4], V.M. Placco[4], J. Yoon[4], and L.A. Buchhave[5,6]

[1] Observatories of the Carnegie Institution of Washington, 813 Santa Barbara St., Pasadena, CA 91101
e-mail: thansen@carnegiescience.edu
[2] Dark Cosmology Centre, The Niels Bohr Institute, University of Copenhagen, Juliane Maries Vej 30, DK-2100 Copenhagen, Denmark
e-mail: ja@astro.ku.dk, birgitta@astro.ku.dk
[3] Stellar Astrophysics Centre, Department of Physics and Astronomy, Aarhus University, DK-8000 Aarhus C, Denmark
[4] Department of Physics and JINA Center for the Evolution of the Elements, University of Notre Dame, Notre Dame, IN 46556, USA
e-mail: tbeers@nd.edu,vplacco@nd.edu,jyoon4@nd.edu
[5] Harvard-Smithsonian Center for Astrophysics, Cambridge, MA 02138, USA
[6] Centre for Star and Planet Formation, University of Copenhagen,DK-1350 Copenhagen, Denmark
e-mail: buchhave@astro.ku.dk

ABSTRACT

Context. Detailed spectroscopic studies of metal-poor halo stars have highlighted the important role of carbon-enhanced metal-poor (CEMP) stars in understanding the early production and ejection of carbon in the Galaxy and in identifying the progenitors of the CEMP stars among the first stars formed after the Big Bang. Recent work has also classified the CEMP stars by absolute carbon abundance, A(C), into high- and low-C bands, mostly populated by binary and single stars, respectively.

Aims. Our aim is to determine the frequency and orbital parameters of binary systems among the CEMP-*s* stars, which exhibit strong enhancements of neutron-capture elements associated with the *s*-process. This allows us to test whether local mass transfer from a binary companion is necessary and sufficient to explain their dramatic carbon excesses.

Methods. We have systematically monitored the radial velocities of a sample of 22 CEMP-*s* stars for several years with ∼monthly high-resolution, low S/N échelle spectra obtained at the Nordic Optical Telescope (NOT) at La Palma, Spain. From these spectra, radial velocities with an accuracy of ≈ 100 m s^{-1} were determined by cross-correlation with optimized templates.

Results. Eighteen of the 22 stars exhibit clear orbital motion, yielding a binary frequency of 82±10%, while four stars appear to be single (18±10%). We thus confirm that the binary frequency of CEMP-*s* stars is much higher than for normal metal-poor giants, but *not* 100% as previously claimed. Secure orbits are determined for 11 of the binaries and provisional orbits for six long-period systems ($P > 3,000$ days), and orbital circularisation time scales are discussed.

Conclusions. The conventional scenario of local mass transfer from a former AGB binary companion does appear to account for the chemical composition of *most* CEMP-*s* stars. However, the excess of C and *s*-process elements in *some single* CEMP-*s* stars was apparently transferred to their natal clouds by an external (distant) source. This finding has important implications for our understanding of carbon enrichment in the early Galactic halo and some high-redshift DLA systems, and of the mass loss from extremely metal-poor AGB stars.

Key words. Galaxy: formation – Galaxy: halo – Stars: chemically peculiar binaries: spectroscopic – ISM: structure.

1. Introduction

Over the past few decades, large spectroscopic surveys have identified numerous very metal-poor (VMP; [Fe/H] < -2.0) and extremely metal-poor (EMP; [Fe/H] < -3.0) stars in the halo system of the Milky Way. High-resolution follow-up spectroscopy has also provided an increasingly detailed picture of the star-to-star elemental-abundance variations that constrain the early chemical evolution of the Galaxy (for reviews, see Beers & Christlieb 2005; Ivezic et al. 2012; Frebel & Norris 2015). The abundance patterns of individual chemically-peculiar stars that deviate markedly from those of the bulk of Population II stars can then be used to identify the nature of the progenitors and nucleosynthetic processes responsible for the production of their distinctive chemical signatures. Dilution of these signatures by later mixing with the interstellar medium (ISM) of the Galaxy ultimately establishes the mean abundance trends for relatively more metal-rich stars.

A key element in this context is carbon, which is found to be over-abundant in a large fraction of VMP stars (≳20% for [Fe/H] ≤ -2). Carbon-enhanced metal-poor (CEMP) stars were originally identified among the VMP and EMP stars discovered in the HK survey of Beers, Preston, & Shectman (Beers et al. 1985, 1992) and the Hamburg/ESO survey of Christlieb and collaborators (Christlieb et al. 2008), and supplemented by a number of surveys since. The fraction of CEMP stars rises with decreasing metallicity (conventionally tracked by the iron abundance, [Fe/H]); hence they are of particular importance for studies of the early chemical evolution of the Galactic halo.

The CEMP stars comprise a number of sub-classes (see Beers & Christlieb 2005). The best-populated of these are the CEMP-*s* and CEMP-no stars, characterised by the presence or

Table 1. Coordinates, photometry, and abundances for the CEMP-*s* and CEMP-*r*/*s* stars monitored for radial-velocity variation

Stellar ID	RA (J2000)	Dec (J2000)	V	$B-V$	Ref$_{Phot}$	[Fe/H]	[C/Fe]	[Ba/Fe]	Ref$_{Abund}$
CEMP-*s*									
HE 0002−1037	00:05:23	−10:20:23	13.70	0.48	a	−3.75	+3.19	+1.67	1
HE 0111−1346	01:13:47	−13:30:50	12.48	1.31	b	−1.91	+1.70	< +2.32	2,1
HE 0151−0341	01:53:43	−03:27:14	13.36	1.14	b	−2.46	+2.46	+1.22	2,1
HE 0206−1916	02:09:20	−19:01:55	14.00	1.13	b	−2.09	+2.10	+1.97	3
HE 0319−0215	03:21:46	−02:04:34	13.79	1.39	b	−2.30	+2.00	+0.52	1
HE 0430−1609*	04:32:51	−16:03:39	13.17	1.25	b	−3.00	+1.14	+1.62	1
HE 0441−0652	04:43:30	−06:46:54	14.23	1.02	b	−2.47	+1.38	+1.11	3
HE 0507−1430	05:09:17	−16:50:05	14.49	1.54	b	−2.40	+2.60	+1.30	4
HE 0507−1653	05:10:08	−14:26:32	12.51	1.13	b	−1.38	+1.29	+1.89	3
HE 0854+0151	08:57:30	+01:39:50	14.98	0.92	b	−1.80	+1.60	+0.82	1
HE 0959−1424	10:02:04	−14:39:22	13.37	0.60	b	−1.42	+2.30	+1.24	1
HE 1031−0020	10:34:24	−00:36:09	11.87	0.74	a	−2.81	+1.58	+1.55	8
HE 1045+0226	10:48:03	+02:10:47	14.10	1.01	a	−2.20	+0.97	+1.24	5
HE 1046−1352	10:48:30	−14:08:12	14.71	0.68	b	−2.76	+3.30	+1.38	1
CS 30301−015	15:08:57	+02:30:19	13.04	1.00	b	−2.64	+1.60	+1.45	7
HE 1523−1155	15:26:41	−12:05:43	13.23	1.35	b	−2.15	+1.86	+1.72	3
HE 2201−0345	22:03:58	−03:30:54	14.31	1.18	b	−2.80	+2.30	+0.62	1
HE 2312−0758	23:14:55	−07:42:32	14.32	1.02	a	−3.47	+1.86	+1.99	1
HE 2330−0555	23:32:55	−05:38:50	14.56	0.85	b	−2.78	+2.09	+1.22	3
CEMP-*r*/*s*									
HE 0017+0055	00:20:22	+01:12:07	11.46	1.53	b	−2.40	+2.17	> +1.99	10
HE 0039−2635**	00:41:40	−26:18:54	12.22	1.12	b	−2.90	+2.63	+2.03	6
LP 624−44	16:43:14	−01:55:30	11.68	1.16	a	−2.72	+2.25	+2.83	9

Notes. * = LP 775−30; ** = CS 29497−034.

References. *Photometry:* a) Henden et al. (2015), b) Beers et al. (2007a). *Abundances:* 1) This work, 2) Kennedy et al. (2011), 3) Aoki et al. (2007), 4) Beers et al. (2007b), 5) Cohen et al. (2013), 6) Barbuy et al. (2005), 7) Aoki et al. (2002b), 8) Cohen et al. (2006), 9) Aoki et al. (2002c), 10) Jorissen et al. (2015a).

absence of enhancements in *s*-process elements in addition to their carbon enhancement. The great majority of the former can be accounted for by scenarios involving transfer of enriched material from a binary companion that has passed through the asymptotic giant-branch (AGB) stage of evolution.

The origin of the latter has still not been identified with certainty, but their binary frequency is not higher than among metal-poor giants in general (see Paper II of this series, Hansen et al. 2015c). As discussed there, a number of lines of evidence strongly suggest that the CEMP-no stars contain the nucleosynthesis products of the very first stars born in the Universe, i.e., that they are bona-fide second-generation stars. A third, less populated, sub-class is the CEMP-*r*/*s* stars (which exhibit enhancements of both *r*-process and *s*-process elements in addition to that of carbon); their origin is presently poorly understood and needs further observational attention.

Lucatello et al. (2005) carried out a limited multi-epoch RV-monitoring survey of 19 CEMP-*s* stars, and by combining with results from previous authors, argued that some 68% of the stars in their sample exhibited evidence for radial-velocity variation. Based on the Duquennoy & Mayor (1991) distributions of orbital elements for Solar-type dwarfs and their simulation of the sampling of phase space by the velocity windows covered in their observations, they concluded that the observations were compatible with 100% of CEMP-*s* stars being members of binary (or multiple) systems. A re-analysis of this sample augmented with new data by Starkenburg et al. (2014) came to a similar conclusion. However, we emphasize that the size of the sample considered, and the range of periods that could be examined based on these data, is still relatively small.

In this series of papers we present the results of an eight-year programme of precise radial-velocity monitoring and prompt, systematic follow-up of potentially variable objects, for larger samples of chemically-peculiar VMP and EMP stars than have heretofore received such close attention. Our goal is to perform a solid test whether the distinctive abundance signatures of these objects can be accounted for by alteration of their birth chemistry by highly-evolved binary companions.

Hansen et al. (2011) first showed that the enhancement of *r*-process elements observed in a small fraction (3-5%) of VMP and EMP stars is *not causally connected* to membership in a binary system, a conclusion that was confirmed and further strengthened in Paper I of this series (Hansen et al. 2015b). Paper II (Hansen et al. 2015c) examined the same question for the class of CEMP-no stars and found that only 17±9% (4 of 24) of their programme stars were binaries, identical to the binary frequency found in metal-poor red giants. The present Paper III addresses the extent to which binaries may play a role in the origin of CEMP-*s* and CEMP-*r*/*s* stars, using the same approach.

This paper is outlined as follows: Section 2 summarises the selection of our programme stars and briefly describes our observational strategy and the techniques employed. Results are presented in Section 3, and Section 4 describes the orbital properties of our binary programme stars. In Section 5, we discuss the constraints imposed by these results on the progenitors of CEMP-*s* stars; a similar discussion for CEMP-*r*/*s* stars is provided in Section 6. Section 7 discusses the significance of the single stars identified in our programme, and Section 8 presents our conclusions and perspectives on what can be learned from future spectroscopic results on CEMP-*s* and CEMP-*r*/*s* stars.

Table 2. Barium and europium abundances for the potential CEMP-*r*/*s* stars in the sample

Stellar ID	[Ba/Fe]	[Eu/Fe]	[Ba/Eu]	Ref
HE 0017+0055	>+1.9	+2.3	>−0.4	Jorissen et al. (2015a)
HE 0039−2635	+2.03	+1.80	+0.23	Barbuy et al. (2005)
HE 1031−0020	+1.55	< +0.82	> +1.27	Cohen et al. (2013)
CS 30301−015	+1.45	+0.20	+1.25	Aoki et al. (2002b)
LP 625−44	+2.83	+1.72	+1.11	Aoki et al. (2002c)

2. Sample selection, observations, and analysis

2.1. Sample definition

Our sample of stars is presented in Table 1, which lists their V magnitudes, $B-V$ colours, and published [Fe/H], [C/Fe], and [Ba/Fe] abundances, either from the literature or determined as described below.

The majority of our programme stars are selected from the Hamburg/ESO survey of Christlieb and collaborators (HES; Christlieb et al. 2008), with the addition of one star from the HK survey, CS 30301−015. The CEMP star LP 625−44 was added since it is well-studied, and previous authors have suggested that it might be a CEMP-*r*/*s* star. Two of the sample stars are re-discoveries; HE 0039−2635 of the HK survey star CS 29497−034, and HE 0430−1609 of the high proper-motion star LP 775−30.

For the stars in Table 1 labelled solely with a '1' in the final column ('this work'), the [Fe/H] and [C/Fe] abundances were determined from medium-resolution (R∼2000) spectra, using the n-SSPP pipeline software (described in detail by Beers et al. 2014). These candidates were selected from the CEMP candidate lists of Placco et al. (2010, 2011), and earlier spectroscopic follow-up of HES candidates over the last 25 years. These stars would clearly benefit from higher-resolution spectroscopic abundance analyses.

Additionally a number of stars in our programme had no abundance estimate (or upper limit) barium available in the literature; the [Ba/Fe] abundance is required in order to make a confident assignment of a star into the CEMP-*s* sub-class. For these stars we have derived Ba abundances (or upper limits) from our co-added high-resolution spectra, following the procedure described in Paper II. This exercise clearly confirms the classification of all of these stars as CEMP-*s* stars (see Table 1).

Four stars in our sample, HE 0039−2635, HE 1031−0020, CS 30301−015, and LP 625−44, have been suggested in the literature to be CEMP-*r*/*s* stars: Carbon stars showing enhancement in both *r*- and *s*-process elements ($0.0 <$ [Ba/Eu] $< +0.5$; Beers & Christlieb 2005). Additionally, during the preparation of this paper, Jorissen et al. (2015a) discovered that HE 0017+0055 also has a very high Eu abundance. Table 2 lists the Ba and Eu abundances for all these stars, along with their [Ba/Eu] ratios. The very high Eu abundance of HE 0017+0055, combined with the lower limit on its Ba abundance, cause its [Ba/Eu] ratio to fall below the above formal limit. In summary, only HE 0039−2635 fully qualifies as a CEMP-*r*/*s* star; nevertheless, Eu is detected in the three other stars of the sample and should be accounted for in any formation scenarios of the CEMP-*r*/*s* stars, which are discussed more fully in Sect. 6.

In the remainder of this paper, we retain the CEMP-*r*/*s* label for HE 0039−2635, HE 0017+0055 and LP 625−44. However, because the Eu abundance of HE 1031−0020 is only an upper limit and CS 30301−015 has only modestly-enhanced Eu, [Eu/Fe] = +0.20, we discuss these stars together with the other CEMP-*s* stars.

2.2. Observing strategy

The key scientific goal of our project was to identify the single and binary stars in the sample and, if possible, determine the orbital periods and eccentricities with sufficient precision to understand the general properties of each class of stars. Accordingly, our observing strategy throughout the programme was to monitor the radial velocities of the sample stars regularly, precisely, and systematically in a homogeneous manner over a sufficiently long time span to detect any spectroscopic binaries among the stars, building on the examples of Duquennoy & Mayor (1991) and Carney et al. (2003).

Maintaining a roughly monthly cadence in the observations was considered adequate for the expected long orbital periods. Aiming for a precision of the individual observations of ~ 100 m s^{-1}, and continuing the observations for up to 2,900 days allowed us to detect orbital motion with very long periods. Moreover, the observations were reduced and the velocities inspected promptly after every observing night, so that any incipient variability could be detected and the observing cadence adapted as appropriate for each target.

As described in Paper I, this strategy enabled us to identify the star HE 1523−0901 as a very low-inclination binary despite its awkward period of 303 days and velocity semi-amplitude of only 0.35 km s^{-1}. This is evidence that we are able to securely detect binary orbits of even very low amplitude, as seen also in the results displayed in Table 4. However, observations of a given star were discontinued when our key scientific objectives had been reached; spending precious telescope time to achieve ultimate precision *per se* was not a priority beyond that point.

2.3. Observations and data analysis

Following the above strategy, the observations, reductions, and analysis procedures were the same as those of Papers I and II of this series, to which the interested reader is referred for details; here we only give a short summary. The stars were observed with the FIES spectrograph at the 2.5m Nordic Optical Telescope (NOT). The spectra cover a wavelength range of 3640 Å to 7360 Å, at a resolving power of $R \approx 46,000$ and average signal-to-noise ratio (SNR) of ≈ 10. Background contamination was minimised by observing the stars in grey time, when the cross-correlation profile peaks of the stellar spectrum and any moonlight spectrum were well-separated in velocity space.

Reductions and multi-order cross-correlations were performed with software developed by L. Buchhave. The template spectra employed for a given target were either the spectrum of the star with maximum signal ("Strongest"); a Co-added spectrum of all the best spectra ("Co-add"); a Synthetic spectrum consisting of delta functions at the Solar wavelengths of the strongest stellar lines ("Delta"); or a co-added spectrum of a bright CEMP-*s* star (HE 0507−1653) with a spectrum similar to that of the object.

Depending on the average quality of the spectra for a given star (S/N ratio; line density and strengths), the individual spectra were cross-correlated against one of these templates. The "Strongest" or "Co-add" templates were usually preferred, as they give a perfect match to the stellar spectrum and thus allow us to include the largest number of spectral orders in the correlations and optimise the precision of the derived radial velocities. However, for some low-signal spectra it was not possible to use these two templates; a Co-add spectrum of a bright CEMP-*s* star was then used.

The spectra of the CEMP-*s* (and CEMP-*r*/*s*) stars are generally richer in strong lines than those of the *r*-process-enhanced and CEMP-no stars discussed in Papers I and II. Therefore, most stars discussed here could be correlated with the "Strongest" or "Co-add" templates, the same template being used for all spectra of a given star. The typical accuracy of the resulting radial velocities is 1−200 m s^{-1}.

Finally, seven selected radial-velocity standard stars were monitored on every observing night throughout this programme. They are listed in Table 2 of Paper I, which gives the derived mean heliocentric velocities and standard deviations. The mean difference of our measured velocities for these stars from their standard values is 73 m s^{-1} with a standard deviation per star of 69 m s^{-1}, demonstrating that our results are not limited by the stability of the spectrograph.

3. Results

The results of our radial-velocity monitoring of the sample of CEMP-*s* and CEMP-*r*/*s* stars in Table 1 are summarised in Table 3, which lists the number of observations (N_{obs}) for each star, the cross-correlation template used, the resulting mean heliocentric radial velocity (RV_{mean}) and its standard deviation (σ), the observed time span (ΔT), the probability that the velocity is constant ($P(\chi^2)$), and our conclusion whether the star is a binary. The individual radial-velocity observations and their associated internal errors, computed as described in Paper I, are given in Appendix A.

A few stars in our sample have radial velocities reported in the literature. The published measurements and total time spans covered for the four stars without significant radial-velocity variations are listed in Table B.1. However, as these data are few in number and exhibit offsets of up to 1 km-s^{-1} between different sources that cannot be properly evaluated, we have not included them in our computations of $P(\chi^2)$ and the accompanying discussion. For the binary stars, the literature data are reviewed in Sect. 3.3 and included in the orbital solutions when found useful.

3.1. Identifying the single and binary stars

As in Paper II, we have assessed the binary status of each individual star by calculating the standard χ^2 parameter for variability to evaluate the probability, $P(\chi^2)$, that the radial velocity is constant within the observational errors. A 'floor error' or 'velocity jitter' of ~ 100 m s^{-1} has been added in quadrature to the internal error to account for sources of external errors such as guiding or atmospheric dispersion and any intrinsic variability (discussed below). The resulting values of $P(\chi^2)$ are listed in Table 3, and demonstrate that at least eighteen of our programme stars exhibit highly significant radial-velocity variations over the eight-year period of monitoring, in most cases clearly due to orbital motion.

However, the context in which the computed $P(\chi^2)$ values are discussed in this paper is the opposite of that in Papers I and II. There, the underlying hypothesis was that of a general population of constant-velocity (i.e., single) stars with a uniform statistical distribution of $P(\chi^2)$ values between 0.01 and 1.00 (see Nordström et al. 1997, Fig. 4, and Carney et al. 2003, Fig. 2). Here, the default expectation, following Lucatello et al. (2005) and Starkenburg et al. (2014), is that *all* CEMP-*s* (and CEMP-*r*/*s*) stars are binaries (i.e., the frequency is 100%).

Thus, the simulations of Lucatello et al. (2005) and Starkenburg et al. (2014) did in fact only allow them to conclude that the compilation of data available to them (establishing an observed frequency of true binaries of 68±11%) was *compatible with* that hypothesis, but it did not *prove* that it was *true*. Additional assumptions in their simulations were that *(i):* the distributions of periods and other orbital parameters followed those derived by Duquennoy & Mayor (1991) for Solar-type dwarfs, and *(ii):* all significant radial-velocity variations were due to binary orbital motion.

Our finding that four stars in our sample exhibit no signs of any binary orbital motion appears to contradict that assumption, especially since 18 of our 22 stars (82%) are well-established binaries with $P(\chi^2)$ values below 10^{-6}, with secure or preliminary orbits for all but one – an even *higher* fraction of actual binaries than found by Lucatello et al. (2005).

Meanwhile, improvements in spectrograph design and radial-velocity precision has revealed low-amplitude long-term velocity variations in essentially all normal and especially bright giants. Accordingly, the ability to detect binary (and exoplanet!) orbital motions of even very low-amplitude and long- period binaries has not only improved due to reduced observational errors, but it is also becoming increasingly limited by intrinsic variability in the target star itself. Moreover, not all potential binary companions are able to evolve past the AGB stage and transfer *s*-process enriched material to the surviving star, so only binary systems with companions of present-day mass in the white dwarf range of 0.5-1.4 $M_\odot$ (Merle et al. 2015) need concern us here. We therefore discuss the binary status of our potentially single stars separately in the following section.

3.2. The apparently single stars

The four stars in Table 3 that are not established binaries all have $P(\chi^2)$ values well above the limit of $P(\chi^2) = 0.05$, beyond which Carney et al. (2003) considered the stars to be safely single and demonstrated that the distribution of their $P(\chi^2)$ values is flat, as expected (see also Nordström et al. 1997, , Fig. 4). However, as also shown by Lucatello et al. (2005), a value of $Q(\chi^2)$ (= 1 – $P(\chi^2)$) ≳0.02 actually indicates that most of them are in fact more likely to be variable than constant. This by itself does not prove that any such variation is necessarily caused by binary *orbital motion*; it must also exhibit a characteristic, significant, systematic, and well-sampled pattern (see, e.g., Morbey & Griffin 1987) .

This is illustrated in Figure 1, which compares the time histories of the velocities of the four single CEMP-*s* stars in our sample with those of the single stars HE 1410+0213 (a CEMP-no star, Paper II) and HD 20 (an *r*-I star, Paper I). Three of these stars (CS 30301−015, HE 0206−1916, and HD 20) have standard deviations of ≲100 m s^{-1} over their total periods of observation, and none of them exhibits any sign of orbital motion.

As discussed in detail in Paper II, HE 1410+0213 was initially suspected of showing orbital motion with a period near 341 days and semi-amplitude ≲ 300 m s^{-1}, but it did not continue this behaviour and eventually was judged to be a single, pulsating star. From the sample presented in this paper, HE 0017+0055 is

Table 3. Number of observations, adopted templates, mean heliocentric radial velocities and standard deviations, observed time spans, and variability criterion $P(\chi^2)$ for the sample stars

Stellar ID	N_{obs}	Template	RV_{mean} (km-s^{-1})	σ (km-s^{-1})	ΔT (Days)	$P(\chi^2)$	Binary
			CEMP-*s*				
HE 0002−1037	10	Co-add	−31.295	5.957	1066	0.000	Yes
HE 0111−1346	9	Strongest	+40.920	8.404	1044	0.000	Yes
HE 0151−0341	11	Co-add	−35.685	9.136	1012	0.000	Yes
HE 0206−1916	9	Co-add	−199.536	0.121	1044	0.233	No
HE 0319−0215	16	Co-add	−225.782	2.357	2207	0.000	Yes
HE 0430−1609	16	Co-add	+231.821	1.727	1184	0.000	Yes
HE 0441−0652	16	Co-add	−30.647	2.655	2371	0.000	Yes
HE 0507−1430	11	Strongest	+44.802	7.920	1064	0.000	Yes
HE 0507−1653	15	Co-add	+348.280	4.859	2124	0.000	Yes
HE 0854+0151	15	Co-add	+138.297	7.798	1757	0.000	Yes
HE 0959−1424	17	HE 0507−1653	+343.379	0.655	2736	0.000	Yes
HE 1031−0020	22	Co-add	+68.660	1.157	2923	0.000	Yes
HE 1045+0226	6	HE 0507−1653	+131.498	0.280	803	0.223	No
CS 30301−015	18	Co-add	+86.607	0.077	2234	0.883	No
HE 1046−1352	12	Strongest	+79.471	21.250	1812	0.000	Yes
HE 1523−1155	9	Co-add	−42.607	3.781	502	0.000	Yes
HE 2201−0345	27	Co-add	−55.927	3.525	2943	0.000	Yes
HE 2312−0758	11	Co-add	+32.981	3.176	1066	0.000	Yes
HE 2330−0555	17	Co-add	−235.124	0.231	2573	0.543	No
			CEMP-*r*/*s*				
HE 0017+0055	28	Strongest	−80.219	1.168	2943	0.000	Yes
HE 0039−2635	2	Strongest	−47.739	6.136	278	0.000	Yes
LP 625−44	28	Co-add	+35.036	3.348	2667	0.000	Yes

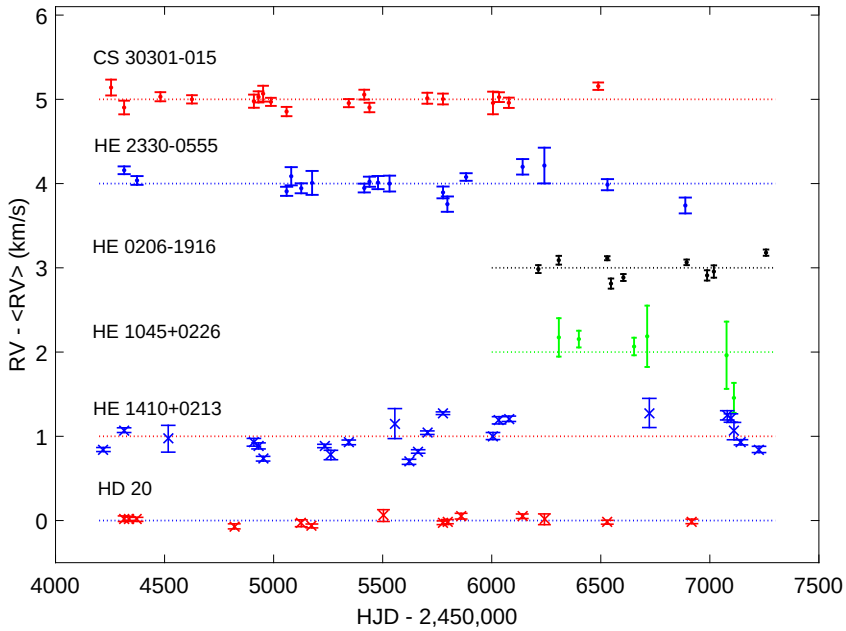

Fig. 1. Observed radial velocities for six constant stars from our project as functions of time, offset by 1 km-s^{-1}. Top to bottom: CS 30301−015, HE 2330−0555, HE 0206−1916, and HE 1045+0226 (this paper); HE 1410+0213 (CEMP-no, Paper II); and HD 20 (*r*-I, Paper I).

found to be a long-period binary (see Table 3), but it also exhibits an additional regular velocity variation of period ≈ 385 days, $e \approx 0.15$, and semi-amplitude $K \approx 540$ m s^{-1}. Finally, in Paper I we found the highly *r*-process enhanced EMP star HE 1523−0901 to be a spectroscopic binary with a period of 303 days and semi-amplitude 350 m s^{-1}.

Adopting these periods and amplitudes, modest orbital eccentricities, and setting $M_1 \approx 0.8$ M$_\odot$ and $M_2 \approx 0.5 - 1.4$ M$_\odot$ for the observed star and the presumed white dwarf companion, respectively, leads to orbital inclinations in the range 1.5° – 2°. Figure 1 suggests that any undiscovered binaries among our four 'single' stars would have periods in the range 1,000−10,000 days

or even longer and semi-amplitudes $\lesssim$ 100 m s^{-1}, leading to similarly low orbital inclinations. Assuming a random distribution of orbits in space, the probability of finding even one such closely face-on orbit is $\approx 10^{-4}$, or less than 1% for our total sample of 63 stars. Having found HE 1523−0901 must then already be considered lucky; finding four such cases strains credulity.

Continued radial-velocity monitoring might still reveal orbital motion in one of our 'constant' stars, notably in HE 1045+0226, but for now, we retain four as the most likely number of single stars, a fraction of 18 ± 10%. Thus, the great majority of the CEMP-*s* stars are still in binaries, but exceptions to the local mass-transfer scenario for their origin do appear to exist, as is the case for the class of CEMP-no stars discussed in Paper II. Alternative scenarios are discussed in Sect. 7.

It is remarkable that two of our CEMP stars (HE 1410+0213 and HE 0017+0055) appear to exhibit near-periodic low-amplitude velocity variations of periods similar to those identified by Riebel et al. (2010) in the large OGLE data set of pulsating LMC giants and C-rich AGB stars. Signatures of similar pulsations in another two CEMP stars are found in the sample of Jorissen et al. (2015b), but not among carbon-normal VMP/EMP *r*-process-enhanced stars. This suggests that the high molecular opacities of C-rich stellar atmospheres may be their source, but photometric confirmation of their existence and probable long periods in field stars is difficult from the ground.

Compounding this difficulty is the lack of reliable distances and absolute luminosities for isolated CEMP stars, and spectroscopic log *g* values are generally uncertain guides due to inadequate resolution of these line-packed spectra. However, the impending precise trigonometric parallaxes and parallel uniform, precise, and well-sampled photometry from the Gaia mission should shortly put our understanding of the properties and evolution of these stars on a much safer footing.

3.3. Binary stars

Radial velocities have been published for a number of our stars that have been found to exhibit variable radial velocities. These data have been included in our discussion of certain or potential binaries in the following.

CEMP-s stars:

- *HE 0111−1346* and *HE 0507−1653* were also observed extensively by Jorissen et al. (2015b), with results agreeing with ours within the errors.

- *HE 0430−1609* and *HE 1523−1155* have suspiciously low rms errors for their orbital solutions. For HE 0430−1609, we can fit eccentric 2,000-day and circular 4000-day orbits to our data, with identical rms errors of only 40 m s^{-1}(!), but consider the latter more reliable (see end note). For HE 1523−1155, the velocities we derived from our observations from 2014 and 2015 plus the observation by Aoki et al. (2007) constrain the period accurately; in particular, much longer periods are excluded despite the significant orbital eccentricity of $e = 0.3$. More observations of these two stars are needed in order to determine the final orbits with confidence.

- *HE 0507−1653* and *HE 1523−1155*: Aoki et al. (2007) has reported single radial velocities for these two objects (353.0 km s^{-1} and −45.0 km s^{-1}, respectively), which fit the orbital solutions derived from our own data; see Figure 3.

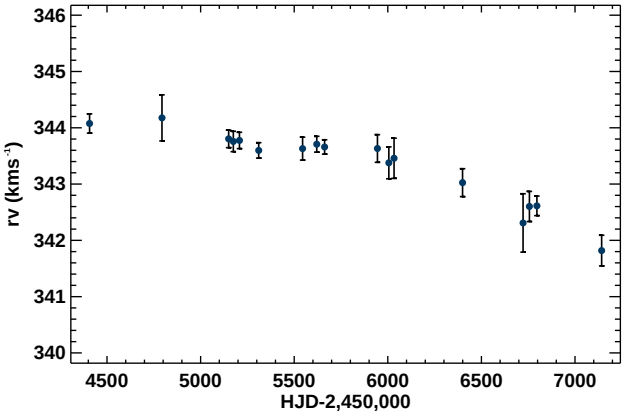

Fig. 2. Radial velocities measured for HE 0959−1424 as function of time, showing a clear decrease over the observing period.

- *HE 0959−1424* undoubtedly has a variable velocity, as indicated by the values of σ and $P(\chi^2)$ given in Table 3. Figure 2 shows the measured radial velocities as a function of time. The slow, systematic velocity decrease suggests that HE 0959−1424 is a binary with a very long period, possibly of the order of 10,000 days or even (much) longer, and a semi-amplitude of a few km s^{-1}. Low-amplitude short-term velocity oscillations of the type seen in HE 0017+0055 are not observed in this star.

CEMP-r/s stars:

- *HE 0017+0055* was monitored extensively in parallel with this programme by Jorissen et al. (2015a), who also discovered its large enhancement of Eu and other *r*-process elements. We have therefore moved it to the CEMP-*r*/*s* subgroup of the sample. Moreover, the analysis of our joint data set revealed a low-amplitude, short-period oscillation superimposed on a highly significant long-term trend. For the short-term oscillation, a Keplerian orbit was formally derived from data covering ≈ 8 full cycles, but the tiny $f(m)$ of $(6\pm1)\times10^{-6}$ M$_\odot$ implied an implausibly low orbital inclination of ≈ 2° (see Sect. 3.2).
  An alternative interpretation in terms of stellar pulsations, based on the complete material, was therefore discussed by Jorissen et al. (2015a), who found the oscillations in this star to be similar to those in the CEMP-no star HE 1410+0213 (Paper II). In the end, regardless of the ultimate cause of these short-period, low-level oscillations, the reality of the long-term orbital motion of HE 0017+0055 is not in doubt, and we retain the star as a binary in our sample.

- *HE 0039−2635* (alias *CS 29497−034*) was observed by both Lucatello et al. (2005) and Barbuy et al. (2005). The former report one measurement from 2002, while the latter reported 11 independent measurements over a span of ≈ 3,000 days between 1995 and 2004 with an rms of 3.4 km s^{-1}, and derived an orbital solution with $P = 4,130$ days and $e = 0.2$. We have combined our results with the published data and find a more eccentric orbit with a shorter period ($P = 3,223$ days, $e = 0.46$); see Figure 4 and Table 4.

- *LP 625−44* has published radial-velocity data from the following sources: Norris et al. (1997): Five observations during 1988−1996; Aoki et al. (2000): Two observations from

Table 4. Orbital parameters for the binary systems in our sample (mean errors are given below each parameter

Parameter	Period	T_0	K	γ	e	ω	$a \sin i$	$f(m)$	M_2	R_{Roche}	σ
Units	(days)	(HJD)	(km s^{-1})	(km s^{-1})		(°)	($R_\odot$)	($M_\odot$)	($M_\odot$)	($R_\odot$)	(km s^{-1})
CEMP-s Stars											
HE 1046−1352	20.156	51,199.88	30.19	+75.37	0.00	0	12.03	0.057	0.4	5.8	0.82
	0.001	0.04	0.30	0.16	0.00	—	0.01	0.008	1.4	22.0	
HE 1523−1155	309.34	57,009.3	5.21	−42.94	0.272	100	30.66	0.0040	0.4	31.9	0.018
	0.62	2.6	0.04	0.11	0.008	2	0.18	0.0002	1.4	132.5	
HE 0151−0341	359.07	55,313.4	12.15	−37.74	0.00	0	86.22	0.0667	0.45	42.2	0.08
	0.21	0.7	0.03	0.03	0.00	—	0.16	0.0004	1.4	146	
HE 0854+0151	389.85	55,305.58	12.86	+133.58	0.00	0	99.1	0.0859	0.5	52.0	0.13
	0.07	0.07	0.03	0.02	0.00	—	0.1	0.0003	1.5	155	
HE 0111−1346	403.81	56,320.2	12.74	+37.75	0.00*	0	101.32	0.8855	0.55	56.7	0.11
	0.14	0.1	0.02	0.02	—	—	0.08	0.0001	1.4	162	
HE 0507−1653	404.18	55,840.24	7.090	+349.843	0.00	0	56.63	0.0145	0.4	36	0.20
	0.05	0.07	0.008	0.006	0.00	—	0.03	0.0002	1.4	156	
HE 0507−1430	446.96	55,272.71	10.927	+42.961	0.0058	84	96.64	0.0604	0.44	47	0.05
	0.15	0.16	0.011	0.009	0.0015	11	0.06	0.0001	1.4	169	
HE 0002−1037	740.9	56,622.5	9.50	−32.49	0.142	85	138.0	0.064	0.4	67	0.29
	1.0	0.5	0.08	0.03	0.005	3	0.5	0.003	1.4	242	
HE 2312−0758	1,890	56,536	4.33	+33.16	0.26*	0	156	0.014	0.4	99	0.14
	57	7	0.08	0.15	—	—	6	0.005	1.4	447	
HE 0319−0215	3,078	53,572	4.28	227.23	0.00	0	260.3	0.025	0.4	142	0.34
	25	19	0.05	0.05	0.00	—	3.2	0.05	1.4	634	
HE 1031−0020	3,867	56,006	1.78	+68.22	0.38*	245	126	0.002	0.6	284	0.17
	175	54	0.07	0.06	—	—	28	0.035			
HE 0430−1609	4,368	58,873	3.80	+231.15	0.0*	0	328	0.025	0.6	310	0.04
	198	96	0.15	0.06	—	—	20	0.002			
HE 0441−0652	5,223	58,408	8.7	−34.58	0.48*	217	785	0.24	0.72	540	0.64
	628	308	3.3	1.95	—	—	193	0.26			
HE 2201−0345	10,093	55,696	5.13	−58.08	0.67	28	749	0.055	0.6	556	0.17
	1,656	8	0.05	0.24	0.04	1	129	0.029			
CEMP-r/s Stars											
HE 0039−2635	3,223	51,900	6.9	−46.5	0.46*	239	424	0.09	0.6	264	1.32
	36	12	0.5	10.4	—	—	139	0.53			
HE 0017+0055	3,529	55,407	1.57	−80.39	0.43	312	99	0.001	0.6	64	0.33
	236	40	0.06	0.05	0.05	8	9	0.035			
LP 625−44	4,863	56,007	6.35	+33.63	0.35*	245	571	0.10	0.6	332	0.42
	12	16	0.04	0.06	—	—	18	0.01			

Notes. * Eccentricity fixed in the solution.

1998−2000; and Lucatello et al. (2005): Three observations from 2000−2002. None of these authors had sufficient data to compute an orbital solution for this star. However, combining their data with our own extensive series of measurements, and applying offsets between the literature velocities and ours (Norris et al., −0.14 m s^{-1}; Aoki et al., +451.96 m s^{-1}; and Lucatello et al., +155.87 m s^{-1}), we could construct a data set covering a total time span of 9,582 days. From this, we have computed an orbit with a period of $P = 4,863$ days and $e = 0.35$; see Table 4 and Figure 4.

4. Binary orbital solutions

Orbital solutions have been obtained for the 17 confirmed binary systems in our sample, except the probable (very) long-period binary HE 0959−1424, discussed above. Our final orbital parameters for these 17 systems are listed in Table 4 in order of increasing period, and radial-velocity curves are shown, also in order of increasing period, in Figure 3 for the CEMP-s stars and in Figure 4 for the CEMP-r/s stars.

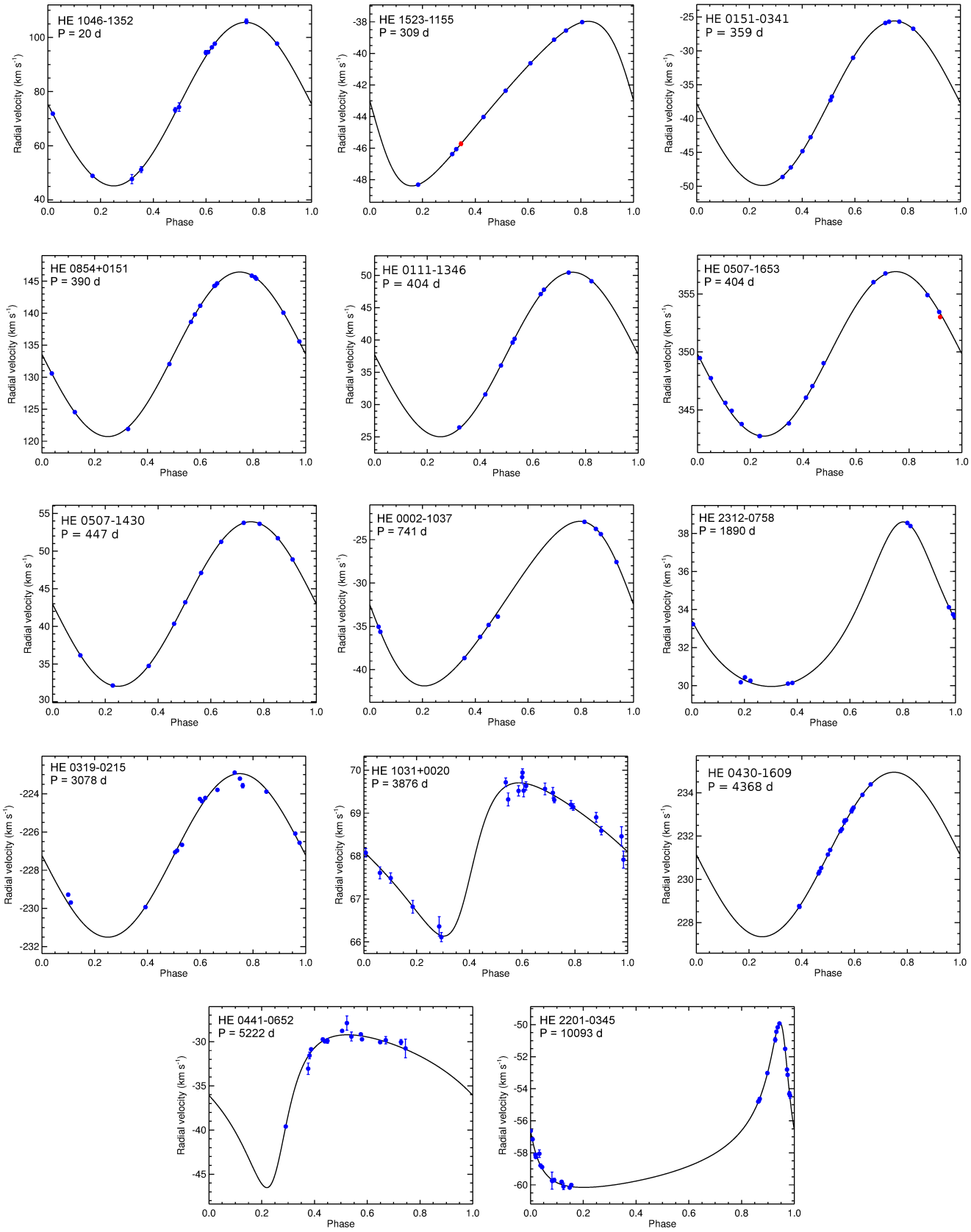

Fig. 3. Orbit solutions for the CEMP-*s* binaries in our programme. Blue symbols: this work; red symbols: Aoki et al. (2007).

The orbital periods of the binaries among our programme stars range from 20 days to ≈ 30 years, the majority having periods around one year; most of these are in circular orbits. Naturally, for orbits with periods in excess of the ≈ 3,000-day time span of our observations, the orbital parameters have correspondingly larger errors.

Table 4 also lists the Roche-lobe radii of the secondary stars in these systems, calculated by the procedure described in Paper I. For this, we have assumed a mass of 0.8 $M_\odot$ for the observed metal-poor giant primary stars, and secondary masses of 0.4 $M_\odot$ (larger if $i = 90°$ is reached) and 1.4 $M_\odot$, respectively (minimum and maximum masses for the presumed white dwarf companion). For orbital periods $P \gtrsim 3{,}000$ days, these Roche-lobe radii become very uncertain; therefore, only indicative values for $M_2 = 0.6$ $M_\odot$ are given.

4.1. Binary fraction and distribution of orbital eccentricities

With seventeen confirmed and one likely binary systems, the binary frequency of our sample is 77−82±10%, taking Poisson sampling errors into account, but ≈ 20% of the stars appear to be single. Thus, the frequency of spectroscopic binaries among CEMP-*s* stars is clearly much higher than among both Population I and II giants in the field (Mermilliod et al. 2007; Carney et al. 2003), but as discussed in Sect. 3.2, it is probably *not quite* the 100% surmised by Lucatello et al. (2005). That ≈ 20% of the stars remain single suggests that, like the CEMP-no stars of Paper II, they did not receive their high carbon and *s*-process-element abundances via mass transfer from a former AGB companion; another scenario must be invoked (see Sect. 7).

Figure 5 shows our binary systems (Table 4) in the period-eccentricity diagram (red plus signs and red and blue triangles), along with comparison samples of 141 giant binary members of open clusters of all ages by Mermilliod et al. (2007) and Mathieu et al. (1990) (black dots), and 16 metal-poor binaries from Carney et al. (2003) (black crosses). HE 0959−1424 has been included in the plot with a fictitious period of 15,000 days to indicate that its period is likely very long, but presently unknown. The three CEMP-*r*/*s* stars (HE 0017+0055, HE 0039−2635, and LP 625−44; blue triangles) have similar eccentric orbits with long periods (of the order a decade or more), and are among the longest-period stars in our sample (Table 4). However, the present sample is too small to claim any difference in binary characteristics between CEMP-*r*/*s* and CEMP-*s* stars (see further discussion in Sect. 6).

The period-eccentricity diagram shown in Figure 5 exhibits the expected overall feature (Jorissen et al. 1998, 2015b) of (near-) circular orbits up to a cutoff that depends on the age of the systems, but can be estimated at ≈ 200 days for Population I and Population II giants of all ages. This is commonly ascribed to tidal circularisation of the orbits, which is more advanced the older the star (the few moderately eccentric shorter-period binaries are probably younger and/or more metal-poor stars in uncertain stages of evolution).

The CEMP-*s* and CEMP-*r*/*s* binaries shown in Figure 5 indicate a cutoff period in the range 500−700 days, suggestive of larger (AGB) secondaries. Two systems, HE 1046−1352 and HE 1523−1155, are exceptions to this general trend. HE 1046−1352, with a period of only 20 days, does have the expected circular orbit, but the calculated Roche-lobe radii for an average-mass white dwarf secondary are too small to accommodate even a normal giant star, let alone an AGB star of ≈ 200 $R_\odot$. HE 1046−1352 could be a misclassified dwarf or the result of a common-envelope phase of evolution, similar to the even shorter-period system HE 0024−2523 discussed by Lucatello et al. (2003) on the basis of its high spectroscopic log *g*, remarkable abundance pattern, and high rotation.

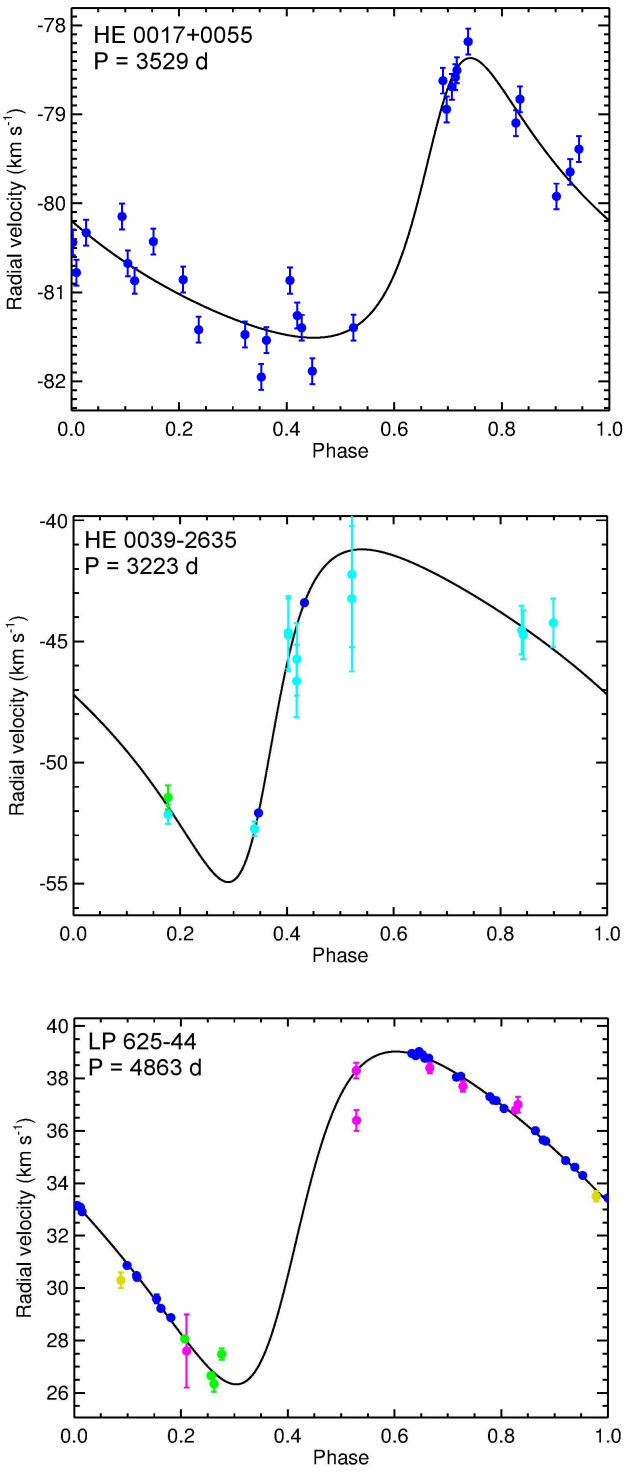

Fig. 4. Orbits for the CEMP-*r*/*s* stars. Symbols: Blue: this work; magenta: Norris et al. (1997); green: Lucatello et al. (2005); yellow: Aoki et al. (2000); light blue: Barbuy et al. (2005).

HE 1523−1155 deviates from expectation in the opposite sense, in that it has a highly significant eccentricity of $e = 0.3$, yet has a shorter period (309 days) than the ≈ 600-day cutoff

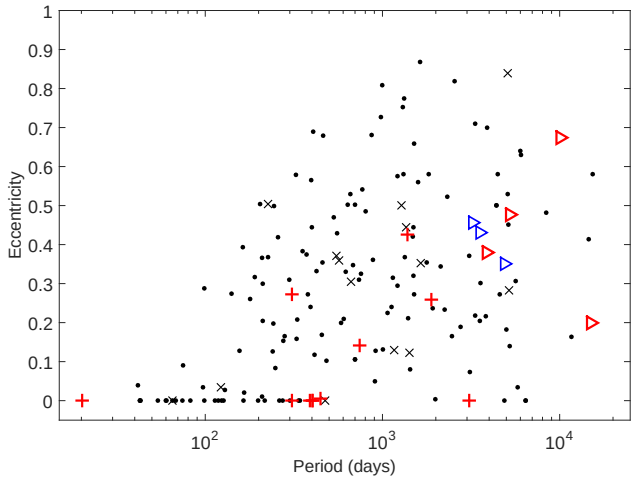

Fig. 5. Period−eccentricity diagram for the binary systems in our sample. Red and blue symbols denote CEMP-*s* and CEMP-*r*/*s* stars, respectively. Systems with periods $P < 3,000$ days are plotted as right-pointing triangles to indicate that the orbital parameters are still uncertain – their periods, in particular, may well be even longer. *Black dots and crosses:* Comparison sample of 141 giant binary members of Galactic open clusters of all ages (Mermilliod et al. 2007; Mathieu et al. 1990) and 16 metal-poor and C-normal binaries from Carney et al. (2003).

defined by the several systems with circular orbits and periods near 500 days. As noted above, the period is observationally strongly constrained, so any additional observations could only confirm the currently derived eccentricity or lead to an even higher value. One might suspect whether HE 1523−1155 could also be a dwarf. However, the spectroscopic $\log g = 1.6$ derived by Aoki et al. (2007) from a Subaru spectrum with $R \approx 50,000$ indicates a giant classification for this star.

5. Formation of CEMP-*s* stars via mass transfer

In analogy with the higher-metallicity CH and Ba stars, and based on recent detailed models for them (e.g., Abate et al. 2015a and references therein), CEMP-*s* stars can be produced through local mass transfer from an AGB binary companion. However, challenges for this scenario remain, such as: (*i*) Can models account for their observed frequencies at low metallicity? (previous attempts fall well short of matching the observations, but progress is being made, see Abate et al. 2015b); (*ii*): Can the models reproduce the observed distribution of periods and (final) separations of the binary components?, and (*iii*): Can the models account for the detailed abundance patterns of CEMP-*s* (and CEMP-*r*/*s*) stars? Final resolution of these questions will require substantially larger samples of CEMP-*s* (and CEMP-*r*/*s*) stars with precise long-term RV-monitoring and high-SNR, high-resolution spectra. Below we speculate on what can be inferred from the present sample.

5.1. Mass-transfer mechanisms

The transfer of mass from an AGB companion star onto the low-mass star we observe today as a CEMP-*s* star can happen in three more-or-less efficient ways: Roche-lobe overflow (RLOF), wind transfer, or wind-assisted Roche-lobe overflow (WRLOF).

Roche-lobe overflow occurs when a binary component expands beyond its Roche-lobe radius. Mass can then be transferred to the companion through the inner Lagrangian point (L1). This is the most efficient way to transfer mass in a binary system, but for RLOF to operate, the separation of the two stars in the system must be relatively small; if the stars are too far apart, neither of them will ever fill its Roche lobe. On the other hand, if the stars are too close, they will enter a common-envelope phase. If a binary system undergoes RLOF, this will circularise the orbit very effectively; even more so if it enters a common-envelope phase. RLOF from stars with large convective envelopes, such as AGB stars, is generally believed to be unstable and often develops into a common-envelope phase (Kopal 1959; Paczyński 1965, 1976). Mass transfer during the common envelope phase is very inefficient and usually considered to be negligible (Ricker & Taam 2008); therefore, RLOF is generally not considered a possible formation mechanism for CEMP-s stars.

From Table 4, it appears that the calculated secondary Roche-lobe radii for our binary systems are only large enough to accommodate an AGB star of ≈ 200 R$_\odot$ in systems with orbital periods $P \gtrsim 1,000$ days and massive present-day WD companions. This, along with the obstacles of common-envelope evolution as mentioned above, would seem to rule out the direct RLOF of mass transfer in shorter-period binaries and favour the WRLOF mode discussed below.

Another method for mass transfer in a binary system is wind transfer, where the low-mass star is exposed to the wind of the AGB star, and can thereby accrete mass (Bondi & Hoyle 1944). This Bondi-Hoyle-Lyttleton (BHL) model of wind mass transfer assumes that the wind of the AGB star does not interact with the orbit of the accreting star, which requires the wind velocity (v_{wind}) to be much higher than the orbital velocity (v_{orbit}); thus, this type of mass transfer is an option only if $v_{wind} >> v_{orbit}$.

This is not always the case for wide binary systems, however. If $P \approx 10^4$ days, the orbital velocity is ≈ 10 km s^{-1}, and the wind from AGB stars can have velocities of 5-30 km s^{-1} (Vassiliadis & Wood 1993). Boffin & Jorissen (1988) explored the possibility of creating Ba stars (the higher-metallicity equivalent of CEMP-*s* stars) via wind transfer in detached binary systems using the BHL wind-accretion scenario, and they concluded that the Ba stars could indeed have been formed in this way. This type of mass transfer allows orbital periods to remain long and orbits to not be circularised.

A third option is the WRLOF mass-transfer mechanism, which can occur in systems where the wind of the donor star is gravitationally confined to the Roche-lobe of the accreting star. The wind can then be focussed towards the orbital plane of the binary system and transferred to the secondary through the L1 point. This type of transfer can be significantly more efficient than BHL wind transfer (Mohamed & Podsiadlowsky 2007). The WRLOF mechanism facilitates mass transfer in binary systems that are too wide for mass transfer via conventional RLOF. The majority of the material that is not accreted by the secondary is lost through the outer Lagrangian points (L2 and L3), and thus carries away angular momentum from the system, shrinking the orbit (Abate et al. 2013).

Abate et al. (2015a) attempted to reproduce the chemical abundance pattern and orbital properties of 15 known CEMP-*s* binary systems. To do this, they compared two models: (1) a WRLOF model with angular momentum loss calculated assuming a spherical symmetric wind, and (2) an enhanced BHL wind-transfer model with efficient angular momentum loss.

Depending on the specific model adopted for the angular-momentum loss, the binary system can widen or shrink in response. Models with WRLOF and a spherically-symmetric wind widen the orbit as mass is transferred, i.e., small initial periods

and consequently small secondary masses are required. Otherwise, they would overflow their Roche lobes, which would lead to a common-envelope phase with no accretion onto the companion. Because the WRLOF is not very efficient for small separations, only small amounts of material is transferred, and this model fails to match the measured abundances of the CEMP-*s* stars.

In contrast, the BHL wind-transfer model with enhanced angular-momentum loss predicts high accretion efficiency (also for systems with relatively short periods), and the enhanced angular-momentum loss ensures that the systems always shrink in response to the mass loss. Thus, even systems that are initially very wide can end up being relatively close when the primary has become a white dwarf.

The majority of their CEMP-*s* binary systems were best reproduced by the second model – a model the authors doubted is realistic, but which emphasized the need for very efficient mass transfer to create the abundance patterns observed in the CEMP-*s* stars. The systems modelled by Abate et al. (2015a) have periods ranging between 3.33 and 4,280 days, and they find initial periods of 1,170 to 130,000 days for these systems.

Hence, Abate et al. (2015a) conclude that, to reproduce the observations, "... it is generally necessary that the modelled binary systems lose efficiently angular momentum and transfer mass with high accretion efficiency." In some systems, a common-envelope phase is even needed to shrink the orbits to their current size. This is particularly true for the binary system HE 0024−2523, with a period of only 3.41 days (Lucatello et al. 2003).

5.2. Nucleosynthesis challenges

Aside from the challenges of efficiently transferring mass in a binary system, most AGB models also face difficulty in reproducing the detailed elemental-abundance patterns found in CEMP-*s* stars. For instance, Bisterzo et al. (2012) fitted the abundance patterns of 94 individual CEMP-*s* and CEMP-*r*/*s* stars with yields from AGB-star models. The outcome of that exercise demonstrated that the models have problems reproducing the C and N abundances, as well as the $^{12}C/^{13}C$ ratios reported for CEMP stars. Carbon is generally over-produced in their models. Combined with the observed low $^{12}C/^{13}C$ ratios (see, e.g., Ryan et al. 2005 and Hansen et al. 2015a, and references therein), this points toward a large amount of mixing not being included in their models. Recent work by Abate et al. (2015a) and Abate et al. (2015b), employing models of AGB nucleosynthesis production from Karakas (2010), reaches better agreement for some stars, while for others they have the same problem as Bisterzo et al. (2012).

In addition, predictions of the *s*-process-element distributions present difficulties. The AGB models of Bisterzo et al. (2012) predict roughly similar abundances (within 0.3 dex) of the first-peak (Sr, Y, Zr) and second-peak elements (Ba, La, Ce, Pr, and Nd), while the derived abundances for CEMP-*s* stars exhibit an internal spread in these elements of more than 0.5 dex. Barium is often found to be more enhanced than the other second-peak elements.

Placco et al. (2013) attempted to match the measured abundances of CEMP-*s* stars (without scaling the pattern to the Ba abundance) with yields from the AGB models of Karakas (2010), taking into account the dilution across the binary system. In this case, the elements from the first *s*-process peak were under-produced, while Ba and Pb were over-produced by the model. Alternatively, Hansen et al. (2015a) compared yields from the F.R.U.I.T.Y database of Cristallo et al. (2009, 2011) to the measured abundance pattern of two CEMP-*s* stars. These models failed to reproduce the large amounts of C and N detected in the stars, and also have problems matching the abundances derived for the light neutron-capture elements (Sr, Y, and Zr) of the stars.

Near-ultraviolet (NUV) observations of CEMP-*s* stars also help constrain the theoretical models. Placco et al. (2015) studied two bright CEMP-*s* stars with HST/STIS spectra, which allowed them to determine abundances for elements such as Ge, Nb, Mo, Lu, Pt, and Au. They also matched the abundance pattern with the latest models from Abate et al. (2015a), which take into account not only the AGB evolution, but also the dynamics of the binary system. Even though NUV abundance determinations for CEMP stars are challenging to obtain, they are important inputs for such model-matching exercises.

5.3. Dilution of the accreted material

The accreted material also mixes with interior material from the accreting stars via thermohaline mixing (Stancliffe et al. 2007), which will result in dilution of the accreted material and a change in its abundance pattern. Attempts to model this effect have been made, but the degree to which the transferred material is diluted on the surface of the receiving star is still very poorly constrained (Stancliffe et al. 2007; Stancliffe & Glebbeek 2008).

The accreted material will also be mixed with the material of the accreting star during any dredge-up episodes that occur as the low-mass CEMP-*s* star evolves past the main-sequence stage. This is the case for some of the stars modelled by Abate et al. (2015a), which need to have even more mass transferred to account for the mixing occurring during first dredge-up in order to match the abundance pattern of the observed CEMP-*s* star. In addition, Richard et al. (2002) argue that the degree of dilution depends on the chemical composition of the accreted material. These different mixing effects change the composition of the surface of the CEMP-*s* star, and introduce yet another source of uncertainty into the mass-transfer models.

6. The CEMP-*r*/*s* stars

Europium has been detected in four stars of our sample (see Table 2), indicating an enhancement in *r*-process as well as *s*-process elements. One of these, CS 30301−015, we have now classified as a CEMP-*s* star; it is also a single star. The other three, HE 0017+0055, HE 0039−2635, and LP 625−44, are classified as CEMP-*r*/*s* stars and are long-period binaries with orbital properties that are indistinguishable from those of CEMP-*s* stars.

Based on Ba and Eu abundances for CEMP-*s* and CEMP-*r*/*s* stars, Lugaro et al. (2012) argued that the abundance patterns found for the stars cannot come from the same single AGB star source, essentially opposite to the claim by Allen et al. (2012) that the astrophysical origin of the CEMP-*s* and CEMP-*r*/*s* stars is one and the same.

It has also been speculated that the CEMP-*r*/*s* stars may exhibit the chemical signature of a different origin, the intermediate neutron-capture (*i*-)process. The *i*-process, operating at neutron fluxes between the *s*- and *r*-process, was first proposed by Cowan & Rose (1977) to occur in evolved red giants. This was supported by Masseron et al. (2010), who argued that CEMP-*r*/*s* stars could be the result of mass transfer from more massive AGB stars, where the neutron source $^{22}Ne(\alpha,n)^{25}$ is active

Table 5. Orbital elements for CEMP-r/s binary stars from the literature

Stellar ID	Period	e	Ref
CS 22948−027	427	0.02	Barbuy et al. (2005)
CS 29497−030	346	0.30	Preston & Sneden (2000)
HD 224959	1273	0.18	McClure & Woodsworth (1990)

Table 6. Stellar parameters for single stars

Stellar ID	$T_{\rm eff}(K)$	$\log g$	[Fe/H]	Ref
HE 0206−1916	5200	2.7	−2.09	Aoki et al. (2007)
HE 1045+0226	5077	2.2	−2.20	Cohen et al. (2013)
HE 2330−0555	4900	1.7	−2.78	Aoki et al. (2007)
CS 30301−015	4750	0.8	−2.64	Aoki et al. (2002b)

during the thermal pulses. This source is predicted to produce sufficiently high neutron exposures to not only synthesize elements traditionally associated with the *s*-process, but also elements such as Eu, which are normally associated with the *r*-process (Goriely & Siess 2005). More recently, Bertolli et al. (2013) also found that the abundance pattern of CEMP-r/s stars could be matched with the yields from the *i*-process, thought to occur in high-mass "super-AGB" stars.

We have searched the literature for CEMP stars with *r*- and *s*-process element abundances such that they would qualify as CEMP-r/s stars, and with published radial-velocity data. Nine such stars show radial-velocity variations, but only three have published orbital elements (see Table 5); five show no variation. However, the information on their stage of evolution (essentially a spectroscopic log g) is ambiguous.

Accordingly, no significant new information can be derived from a *P*-*e* diagram such as that in Figure 5, except that the orbital periods of the certified giant CEMP-r/s stars are long and their eccentricities are significant, but moderate – very similar to those of the rest of the CEMP-r/s stars. Larger samples of CEMP-r/s stars with detailed information on binary orbital parameters and a more complete inventory of heavy neutron-capture elements are clearly required for further progress.

7. Composition of the single stars

Four stars in our sample exhibit constant velocities over our observing period, and are judged to be single (see Fig. 1 and Sect. 3.2): HE 0206−1916, HE 1045+0226, HE 2330−0555, and CS 30301−015. The atmospheric parameters for these single stars are listed in Table 6. They are all giants, which may have experienced a first dredge-up (FDU) episode. During this FDU, H, He, and products of the CN cycle are mixed to the surface, resulting in a small decrease in [C/Fe] along with an increase in [N/Fe] at the surface of the star (the precise abundance changes depend on the mass and metallicity of the star and the extent of the FDU, see e.g. Karakas & Lattanzio 2014). Thus, no great change of their surface abundances is expected to have occurred, and a different channel must be invoked to account for the origin of the carbon and *s*-process-element enhancements found in these stars.

To explore this possibility, we have plotted the abundance information we have in common for all of the stars, namely the C, Fe, and Ba abundances; see Figures 6 and 7. The single stars (red dots) exhibit no clear difference in abundance signatures for these elements as compared with the binary stars (blue dots and stars). More detailed abundance analyses, spanning a greater range of elements than is available at present, may reveal differences in the abundance patterns of the single stars vs. those found in binary systems, which could help constrain the likely formation scenario of these stars.

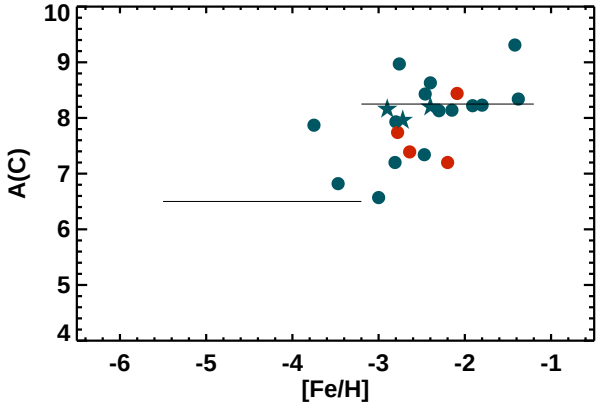

Fig. 6. Absolute C abundances for our programme stars. Dots represent CEMP-*s* stars, star symbols CEMP-r/s stars; red symbols show single stars, blue symbols certified binaries. The two C-bands first noted by Spite et al. (2013) are indicated by horizontal lines.

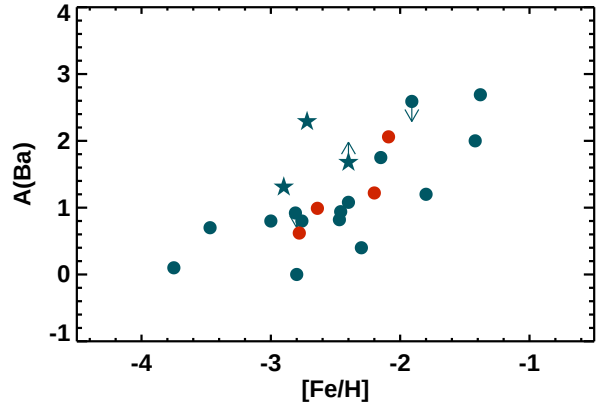

Fig. 7. Absolute Ba abundances for our programme stars. Dots represent CEMP-*s* stars, star symbols CEMP-r/s stars; red symbols show single stars, blue symbols are definite binaries.

7.1. Potential sources of carbon and *s*-process elements in the early Universe

The carbon excess detected in the single CEMP-*s* stars may have a similar origin as the carbon excess seen in the CEMP-no stars, which is believed to be due to either winds from the so-called "spinstars" – massive, rapidly-rotating, metal-free stars (Meynet et al. 2006; Hirschi 2007; Maeder et al. 2015), or to faint supernovae with mixing and fallback as suggested by Umeda & Nomoto (2003).

Spinstars are potentially also a main contributor to *s*-process-element abundances in the early Universe. It was first suggested by Pignatari et al. (2008) that rotation-induced mixing in these stars enhances the production of *s*-process elements via the weak *s*-process. Later, Frischknecht et al. (2012, 2015) explored the

yields of the weak *s*-process in spinstars. They found that mainly light *s*-process elements (Sr, Y, Zr) are produced in this environment, usually with [Sr/Ba] > 0; only in extreme cases does the production run all the way through to Pb.

Abundances of Sr, Ba, and Pb have only been reported in the literature for one of our single stars, CS 30301−015; with [Sr/Ba] = −1.15 and [Pb/Fe] = +1.7 (Aoki et al. 2002b), it does not match the predictions from Frischknecht et al. (2012). On the other hand, detailed models of the abundance patterns generated by spinstars have not yet matured to the point where meaningful star-by-star comparisons can be carried out. Such models might help to identify the progenitors of the single CEMP-*s* stars.

7.2. Carbon bands

Spite et al. (2013) first suggested the existence of two bands in the absolute carbon abundances of CEMP stars – a high-C band at A(C) ≈ 8.25 and a low-C band at A(C) ≈ 6.5. The existence of these two bands for CEMP stars has been confirmed with larger samples by Bonifacio et al. (2015) and Hansen et al. (2015a). The high-C band is primarily populated by relatively more metal-rich stars ([Fe/H] ≳ −3) of the CEMP-*s* sub-class, while the low-C band is primarily populated by more metal-poor stars of the CEMP-no sub-class. While this general behaviour is supported by the CEMP-no (Figure 4 of Paper II), CEMP-*s*, and CEMP-*r*/*s* (Figure 6) stars in our programme, there are clear exceptions. For instance, in Figure 6 a substantial number of stars lie in the transition zone between the two carbon bands, and two stars, classified as CEMP-*s* stars on the basis of their [Ba/Fe] abundance ratios, are nevertheless found close to the low-C band, which is thought to be predominantly associated with CEMP-no stars.

It is remarkable that these stars, HE 0430−1609 and HE 2312−0758, are two of the three lowest-metallicity stars in our sample. Both stars are confirmed binaries with long-period orbits. The presence of these stars on the low C-band could be due to less-efficient mass transfer in these systems. Perhaps no mass-transfer event has occurred in these systems at all, and the CEMP-*s* stars received their C and *s*-process-element excesses from sources similar to the single CEMP-*s* stars. The lowest metallicity CEMP-*s* star in our programme, HE 0002−1037, lies close to the high-C band, similar to the star HE 0959−1424, which is at the high-metallicity limit for stars in our programme and exhibits a carbon abundance that is well above the high-C band.

The single stars in our sample form a heterogeneous group. Three of the stars, HE 1045−0226, CS 30301−015, and HE 2330−0555, lie in the transition zone between the carbon bands, while the fourth, HE 0206−1916, lies on the high-C band.

There clearly remains much work in order to assess the meaning, and possible astrophysical significance, of the suggested carbon bands. Whether this turns out to be a primary behaviour, with deviations that occur for individual stars depending on their precise nucleosynthesis histories, or is correlated with some other factor related to the production and/or dilution of the carbon due to mixing, awaits larger samples with available RV-monitoring and high-SNR spectroscopy.

8. Conclusions

Our systematic and precise long-term radial-velocity monitoring programme of 22 CEMP-*s* and CEMP-*r*/*s* stars has led to a high frequency, 82±10%, of detected binaries in the sample, confirming that the characteristic abundance pattern of the CEMP-*s* stars is coupled to the binary nature of most of these stars. Indeed, it has been taken for granted up to now that *all* CEMP-*s* stars originated from mass transfer in a binary system, a basic assumption which underpins all previous theoretical modelling of these stars.

Four of our programme stars (18%) do, however, appear to be truly single and contradict this basic assumption – as do in fact the entire group of CEMP-no stars discussed in Paper II. This underscores the need for an efficient, distant source of *s*-process elements in the early Universe, whether that source might be spinstars or another class of progenitor. Future detailed abundance analyses of these single stars may reveal signatures in their abundance patterns that will help to constrain the nature of the early C and *s*-process-element production sites and the processes by which these fresh elements were implanted in the natal clouds of the observed CEMP-*s* stars.

For the binary CEMP-*s* stars, we highlight a number of respects, notably the detailed treatment of the physics of the mass transfer process, in which current models still fail to reproduce their observed orbital parameters and elemental abundance patterns.

The three CEMP-*r*/*s* stars in our sample are all long-period binaries, hinting that the origin of these stars is similar to that of the CEMP-*s* stars themselves. However, the available data are much too sparse to be conclusive on such key points as whether their excesses of C and neutron-capture elements stem from the same nuclear source(s), and whether the latter are due to a special form of the *s*-process or to the *i*-process, which has been speculated to operate in the so-called "super-AGB" stars.

Larger samples of binary CEMP-*s* and CEMP-*r*/*s* stars with well-determined orbits, evolutionary status, and detailed abundance patterns are required for further refinement of the theoretical models for the origin of these stars. The accurate trigonometric parallaxes and accompanying precise multi-epoch photometry for many CEMP stars in the field to be expected from the ESA space mission Gaia will soon provide further crucial information on the stage of evolution and pulsational properties of these stars.

Note added in proof: After this paper was accepted, we were able to obtain a final FIES spectrum of HE 0430−1609. Remarkably, this velocity still fits two very different orbits with the same rms error of only 40 m s^{-1}. We retain the longer-period circular orbit as the most likely and have updated the tables and figures accordingly.

Acknowledgements. This paper is based on observations made with the Nordic Optical Telescope, operated by the Nordic Optical Telescope Scientific Association at the Observatorio del Roque de los Muchachos, La Palma, Spain, of the Instituto de Astrofísica de Canarias. We thank numerous NOT staff members and students for readily and very efficiently obtaining most of the many observations for us in service mode. We also thank Carlo Abate for clarifying the response of his modelled binary systems to the different modes of angular-momentum loss. Finally, we thank the anonymous referee for a very careful and incisive report that led to substantive clarifications, revisions and improvements in the paper.
This work was supported by Sonderforschungsbereich SFB 881 "The Milky Way System" (subproject A4) of the German Research Foundation (DFG). J.A. and B.N. gratefully acknowledge financial support from the Danish Natural Science Research Council and the Carlsberg Foundation. T.C.B., V.M.P., and J.Y. acknowledge partial support for this work from grants PHY 08-22648; Physics Frontier Center/Joint Institute or Nuclear Astrophysics (JINA), and PHY 14-30152; Physics Frontier Center/JINA Center for the Evolution of the Elements (JINA-CEE), awarded by the US National Science Foundation.

References

Abate, C., Pols, O. R., Izzard, R. G., Mohamed, S. S., & de Mink, S. E., 2013, A&A, 552, A26
Abate, C., Pols, O. R., Karakas, A., Izzard, R. G., 2015a, A&A, 576, A118

Abate, C., Pols, O. R., Stancliffe, R. J., et al. 2015b, A&A, 581, 62
Allen, D. M., Ryan, S. G., Rossi,S., Beers, T. C., & Tsangarides, S. A. 2012, A&A, 548, 34
Aoki, W., Norris, J. E., Ryan, S. G., Beers, T. C., & Ando, H., 2000, ApJ, L97
Aoki, W., Ryan, S. G., Beers, T. C., & Ando, H., 2002a, PASJ, 54, 933
Aoki, W., Ryan, S. G., Norris, J. E., Beers, T. C., Ando, H., & Tsangarides, S. A., 2002b, ApJ, 580, 1149
Aoki, W., Ando, H., Honda, S., et al., 2002c, PASJ, 54, 427
Aoki, W., Beers, T. C., Norris, J. E., Ryan, S. G., & Tsangarides, S. A., 2007, ApJ, 655, 492
Barbuy, B., Spite, M., Spite, F., et al., 2005, A&A, 429, 1031
Beers, T. C., Preston, G. W.,& Shectman, S. A., 1985, AJ, 90, 2089
Beers, T. C., Preston, G. W.,& Shectman, S. A., 1992, AJ, 103, 1987
Beers, T. C., & Christlieb, N., 2005, ARA&A, 43, 531
Beers, T. C., Flynn, C., Rossi, S., et al., 2007a, ApJS, 168, 128
Beers, T. C., Sivarani, T., Marsteller, B., Lee, Y., Rossi, S., & PLez, B., 2007b, AJ, 133, 1193
Beers, T. C., Norris, J. E., Placco, V. M., et al., 2014, ApJ, 794, 58
Bertolli, M. G., Herwig, F., Pignatari, M., & Kawano, T., 2013, (arXiv:1310.4578)
Bisterzo, S., Gallino, R., Straniero, O., Cristallo, S., & Käppeler, F., 2012, MNRAS, 422, 849
Boffin, H. M. J., & Jorissen, A., 1988, A&A, 205, 155
Bondi, H., & Hoyle, F., 1944, MNRAS, 104, 273
Bonifacio, P., Caffau, E., Spite, M., et al., 2015, A&A, 579, A28
Carney, B. W., Latham, D. W., Stefanik, R. P., et al., 2003, AJ, 125, 293
Christlieb, N., Schörck, T., Frebel, A., et al., 2008, A&A, 484, 721
Cohen, J. G., Christlieb, N., Qian, Y, Z., & Wasserburg, G. J., 2003, ApJ, 588, 1082
Cohen, J. G., McWilliam, A., Shectman, S., et al., 2006, AJ, 132, 137
Cohen, J. G., Christlieb, N., Thompson, I., et al., 2013, ApJ, 778, 56
Cowan, J. J., & Rose, W. K., 1977, ApJ, 212, 149
Cristallo, S., Piersanti, L., Straniero, O., et al., 2011, ApJS, 197, 17
Cristallo, S., Straniero, O., Gallino, R., et al., 2009, ApJ, 696, 797
Duquennoy, A., & Mayor, M., 1991, A&A, 248, 485
Frebel, A., & Norris, J. E., 2015, ARA&A, 53, 631
Frischknecht, U., Hirschi, R., & Thielemann, F.-K., 2012, A&A, 538, L2
Frischknecht, U., Hirschi, R., Pignatari, M., et al., 2015, MNRAS, in press (arXiv 1511.05730)
Goriely, S., & Siess, L., 2005, IAU Symposium 228, From Lithium to Uranium: Elemental Tracers of Early Cosmic Evolution, ed. Hill, V., Francois, P., & Primas, F., 451
Hansen, T., Andersen, J., Nordström, B., Buchhave, L., & Beers, T. C., 2011, ApJ, 743, L1
Hansen, T. T., Hansen, C. J., Christlieb, N., et al., 2015a, ApJ, 807, 173
Hansen, T. T., Andersen, J., Nordström, B., et al., 2015b, A&A, 583, 49 (Paper I)
Hansen, T. T., Andersen, J., Nordström, B., et al., 2015c, A&A, in press (arXiv 1511.08197) (Paper II)
Henden, A. A., Levine, S., Terrell, D., & Welch, D. L., 2015, American Astronomical Society Meeting Abstracts, 225, 336.16
Hirschi, R., 2007, A&A, 461, 571
Ivezic, Z., Beers, T. C., & Juric, M. 2012, ARA&A, 50, 251
Jorissen, A., Van Eck, S., Mayor, M., & Udry, S., 1988, A&A, 332, 877
Jorissen, A., Hansen, T., Van Eck, S., et al., 2015a, A&A, in press (arXiv 1510.06045)
Jorissen, A., Van Eck, S., Van Winkel, H., et al., 2015b, A&A, in press (arXiv 1510.05840)
Karakas, A. I. 2010, MNRAS, 403, 1413
Karakas, A. I, & Lattanzio, J. C., 2014, PASA, 31, 30
Kennedy, C. R., Sivarani, T., Beers., T. C., 2011, AJ, 141, 102
Kopal, Z., 1959, Close Binary Systems, The International Astrophysics Series, London: Chapman Hall
Lucatello, S, Gratton, R., Cohen, J. G., et al., 2003, AJ, 125, 875
Lucatello, S., Tsangarides, S. A., Beers, T. C., Carretta, E., Gratton, R. G., & Ryan, S. G., 2005, ApJ, 625, 825
Lugaro, M., Karakas, A. I., Stancliffe, R. J., & Rijs, C., 2012, ApJ, 747, 2
Maeder, A., Meynet, G., & Chiappini, C., 2015, A&A, 576, A56
Masseron, T., Johnson, J. A., Plez, B., et al., 2010, A&A, 509, A93
Mathieu, R. D., Latham, D. W., & Griffin, R. F., 1990, AJ, 100, 1899
McClure, R. D., & Woodsworth, A. W., 1990, ApJ, 352, 709
Merle, T., Jorissen, A., Van Eck, S., Maseron, T., & Van Winkel, H., 2015, A&A, subm. (arXiv 1510.05908)
Mermilliod, J.-C., Andersen, J., Latham, D. W., & Mayor, M., 2007, A&A, 473, 829
Meynet, G., Ekström, S., & Maeder, A., 2006, A&A, 447, 623
Mohamed, S., & Podsiadlowski, P., 2007, Astronomical Society of the Pacific Conference Series, 372, ed. Napiwotzki, R., & Burleigh, M. R., 397
Morbey, C. L. & Griffin, R. F., 1987, ApJ, 317, 343
Nordström, B., Stefanik, R. P., Latham, D. W., Andersen, J., 1997, A&AS, 126, 21
Norris, J. E., Ryan, S. G., & Beers, T. C., 1997, ApJ, 488, 350
Paczyński, B., 1965, Acta Astron., 15, 89
Paczyński, B., 1976, IAU Symposium 73, Structure and Evolution of Close Binary Systems, ed. Eggleton, P., Mitton, S., & Whelan, J., 75
Pignatari, M., Gallino, R., Meynet, G., et al., 2008, ApJ, 687, L95
Placco, V. M., Kennedy, C. R., Rossi, S., et al., 2010, AJ, 139, 1051
Placco, V. M., Kennedy, C. R., Beers, T. C., et al., 2011, AJ, 142, 188
Placco, V. M., Frebel, A., Beers, T. C., et al., 2013, ApJ, 770, 104
Placco, V. M., Beers, T. C., Ivans, I. I., et al., 2015, ApJ, in press (arXiv:1508.05872)
Preston, G. W., & Sneden, C., 2000, AJ, 120, 1014
Preston, G. W., & Sneden, C., 2001, AJ, 122, 1545
Richard, O., Michaud, G., Richer, J., Turcotte, S., Turck-Chièze, S., & Vandenberg, D. A., 2002, ApJ, 568, 979
Ricker, P. M., & Taam, R. E., 2008, ApJ, 672, L41
Riebel, D., Meixner, M., Fraser, O. et al., ApJ, 723, 1195
Ryan, S. G., Aoki, W., Norris, J. E., & Beers, T. C., 2005, ApJ, 635, 349
Spite, M., Caffau, E., Bonifacio, P., et al., 2013, A&A, 552, A107
Stancliffe, R., & Glebbeek, E., 2008, MNRAS, 389, 1828
Stancliffe, R., Glebbeek, E., Izzard, R. G., & Pols., O.R., 2007, A&A, 464, L57
Starkenburg, E., Shetrone, M. D., McConnachie, A. W., & Venn, K. A., 2015, MNRAS, 441, 1217
Tsangarides, S. A., Ryan, S. G., & Beers, T. C., 2003, Astronomical Society of the Pacific Conference Series, ed: Charbonnel, C., Schaerer, D., & Meynet, G., 304, 133
Umeda, H., & Nomoto, K., 2003, Nature, 422, 871
Vassiliadis, E. & Wood, P. R. 1993, ApJ, 413, 641
Yong, D., Norris, J.E., Bessell, M. S., et al., 2013, ApJ, 762, 26

Appendix A: Radial Velocities Measured for the Programme Stars

Table A.1. HE 0002−1037

HJD	RV km s^{-1}	RV$_{err}$ km s^{-1}
2456191.52615	−36.229	0.045
2456241.45815	−33.883	0.184
2456530.70894	−24.359	0.040
2456574.57567	−27.581	0.044
2456647.45601	−35.052	0.081
2456652.37785	−35.635	0.053
2456888.57469	−38.668	0.061
2456956.43565	−34.844	0.076
2457225.65699	−22.941	0.065
2457257.63749	−23.761	0.055

Table A.2. HE 0017+0055

HJD	RV km s^{-1}	RV$_{err}$ km s^{-1}
2454314.67018	−78.622	0.007
2454338.64193	−78.944	0.007
2454373.62240	−78.691	0.009
2454396.53706	−78.583	0.007
2454406.59662	−78.505	0.012
2454480.38681	−78.183	0.012
2454793.48462	−79.098	0.018
2454820.33862	−78.830	0.017
2455059.73646	−79.922	0.008
2455149.47303	−79.647	0.010
2455207.34980	−79.391	0.015
2455415.60806	−80.439	0.009
2455439.59141	−80.778	0.010
2455503.40860	−80.330	0.023
2455738.73436	−80.148	0.008
2455776.68215	−80.675	0.008
2455821.57659	−80.870	0.009
2455944.32531	−80.429	0.011
2456139.71293	−80.857	0.010
2456241.39102	−81.420	0.018
2456545.62665	−81.474	0.011
2456652.41797	−81.951	0.015
2456686.32089	−81.538	0.015
2456840.71823	−80.866	0.028
2456888.54207	−81.261	0.013
2456917.59811	−81.398	0.014
2456987.38131	−81.885	0.009
2457257.57737	−81.396	0.010

Table A.3. HE 0111−1346

HJD	RV km s^{-1}	RV$_{err}$ km s^{-1}
2456213.65944	+50.431	0.022
2456531.67451	+39.604	0.015
2456534.72823	+40.177	0.024
2456574.62161	+47.100	0.015
2456579.62258	+47.786	0.020
2456652.40265	+49.094	0.021
2456893.65246	+31.577	0.018
2456917.61673	+36.046	0.019
2457257.65967	+26.462	0.026

Table A.4. HE 0151−0341

HJD	RV km s^{-1}	RV$_{err}$ km s^{-1}
2456213.70382	−37.298	0.070
2456307.32814	−25.696	0.064
2456518.73462	−47.217	0.041
2456545.65829	−42.753	0.047
2456574.65686	−36.767	0.030
2456603.50990	−31.030	0.042
2456647.48211	−25.892	0.065
2456652.47616	−25.703	0.072
2456685.39340	−26.739	0.065
2456893.72033	−44.812	0.051
2457225.72100	−48.629	0.065

Table A.5. HE 0206−1916

HJD	RV km s^{-1}	RV$_{err}$ km s^{-1}
2456213.68126	−199.551	0.047
2456307.37509	−199.446	0.052
2456529.69669	−199.422	0.024
2456546.73298	−199.723	0.060
2456603.53471	−199.651	0.041
2456893.67497	−199.471	0.033
2456987.43608	−199.626	0.061
2457018.49730	−199.580	0.073
2457257.68120	−199.356	0.037

Table A.6. HE 0319−0215

HJD	RV km s^{-1}	RV$_{err}$ km s^{-1}
2454780.64369	−229.933	0.029
2455126.64403	−227.058	0.024
2455149.51200	−226.974	0.030
2455207.38599	−226.673	0.017
2455415.70963	−224.274	0.023
2455439.67958	−224.389	0.019
2455478.61056	−224.219	0.022
2455620.34838	−223.797	0.026
2455821.65016	−222.893	0.012
2455882.56766	−223.207	0.020
2455915.54130	−223.575	0.117
2456191.63308	−223.890	0.017
2456528.72760	−226.084	0.028
2456578.64692	−226.565	0.018
2456956.69477	−229.280	0.085
2456987.52074	−229.692	0.063

Table A.7. HE 0430−1609

HJD	RV km s^{-1}	RV$_{err}$ km s^{-1}
2456209.69059	+228.767	0.025
2456214.65424	+228.731	0.021
2456529.71626	+230.277	0.020
2456545.73032	+230.365	0.020
2456574.68459	+230.530	0.015
2456685.46062	+231.151	0.018
2456722.36199	+231.359	0.048
2456893.69735	+232.234	0.035
2456917.63747	+232.325	0.033
2456956.76841	+232.672	0.116
2456986.65656	+232.743	0.022
2457076.35811	+233.154	0.086
2457092.34638	+233.248	0.025
2457110.35827	+233.315	0.050
2457257.71794	+233.909	0.029
2457393.47107	+234.389	0.037

Table A.8. HE 0441−0652

HJD	RV km s^{-1}	RV$_{err}$ km s^{-1}
2454705.73510	−39.600	0.154
2455149.58120	−33.053	0.639
2455176.49676	−31.568	0.372
2455207.53305	−30.860	0.149
2455439.70545	−29.741	0.163
2455478.64746	−29.967	0.081
2455531.57019	−29.901	0.271
2455821.67913	−28.773	0.130
2455915.58170	−27.892	0.810
2456005.34969	−29.417	0.507
2456191.66229	−29.167	0.183
2456214.67479	−29.727	0.170
2456574.73303	−30.053	0.135
2456685.48885	−29.826	0.417
2456987.46556	−30.047	0.298
2457076.43392	−30.762	1.056

Table A.9. HE 0507−1430

HJD	RV km s^{-1}	RV$_{err}$ km s^{-1}
2455149.65141	+53.744	0.017
2455176.59963	+53.614	0.027
2455207.45478	+51.698	0.016
2455232.47668	+48.880	0.016
2455478.68157	+40.340	0.029
2455821.73671	+32.139	0.018
2455882.66528	+34.746	0.032
2455944.52431	+43.196	0.044
2455971.41362	+47.094	0.037
2456005.41341	+51.227	0.077
2456213.73374	+36.148	0.030

Table A.10. HE 0507−1653

HJD	RV km s^{-1}	RV$_{err}$ km s^{-1}
2454793.55000	+346.064	0.053
2454820.45944	+349.034	0.025
2455126.69729	+342.750	0.015
2455171.57052	+343.843	0.014
2455207.51291	+347.058	0.018
2455439.72402	+349.472	0.014
2455478.72231	+345.614	0.052
2455503.57008	+343.789	0.046
2455531.52335	+342.751	0.030
2455860.69191	+347.747	0.015
2455892.55739	+344.930	0.117
2456191.75734	+354.904	0.012
2456209.72120	+353.449	0.021
2456531.71198	+356.770	0.018
2456917.65964	+356.020	0.025

Table A.11. HE 0854+0151

HJD	RV km s^{-1}	RV$_{err}$ km s^{-1}
2454516.50743	+135.575	0.033
2454780.70470	+144.261	0.072
2454930.38332	+130.585	0.034
2454964.39430	+124.541	0.054
2455149.73265	+141.161	0.032
2455171.71750	+144.308	0.024
2455174.67146	+144.662	0.041
2455232.52829	+145.394	0.025
2455531.69023	+139.809	0.040
2455620.45671	+145.626	0.041
2455662.42371	+140.074	0.028
2455822.74479	+121.901	0.112
2455915.75991	+138.642	0.129
2456005.48541	+145.867	0.061
2456273.71422	+132.054	0.062

Table A.12. HE 0959−1424

HJD	RV km s^{-1}	RV$_{err}$ km s^{-1}
2454406.77276	+344.076	0.171
2454793.71150	+344.176	0.409
2455149.76314	+343.803	0.156
2455174.72219	+343.757	0.181
2455207.58849	+343.775	0.145
2455310.37042	+343.598	0.137
2455544.72364	+343.630	0.204
2455620.54421	+343.708	0.140
2455662.38833	+343.659	0.128
2455944.56413	+343.632	0.246
2456005.51849	+343.377	0.283
2456033.36757	+343.459	0.357
2456399.38501	+343.025	0.248
2456722.52147	+342.309	0.519
2456756.38762	+342.602	0.268
2456796.37413	+342.613	0.174
2457142.38500	+341.818	0.273

Table A.13. HE 1045+0226

HJD	RV km s^{-1}	RV$_{err}$ km s^{-1}
2456307.69698	+131.672	0.228
2456399.43421	+131.652	0.099
2456652.61751	+131.564	0.104
2456712.67531	+131.685	0.364
2457076.61932	+131.460	0.399
2457110.44369	+130.954	0.178

Table A.14. HE 1046−1352

HJD	RV km s^{-1}	RV$_{err}$ km s^{-1}
2454909.61389	+94.395	0.795
2454930.45563	+97.658	0.147
2454964.43469	+47.693	1.670
2455174.74220	+105.913	0.851
2455232.57334	+96.330	0.147
2455310.39271	+73.223	0.859
2455344.39166	+48.887	0.278
2455554.78013	+94.567	0.543
2455620.51605	+97.700	0.553
2456006.50365	+71.838	0.545
2456033.41230	+51.174	1.102
2456721.61189	+74.268	1.555

Table A.15. CS 30301−015

HJD	RV km s^{-1}	RV$_{err}$ km s^{-1}
2454254.62579	+86.747	0.094
2454314.47889	+86.510	0.081
2454480.79001	+86.638	0.054
2454625.52411	+86.607	0.049
2454909.59318	+86.585	0.078
2454930.71839	+86.636	0.066
2454951.73429	+86.674	0.094
2454987.49075	+86.577	0.048
2455059.37482	+86.462	0.055
2455344.59436	+86.562	0.048
2455415.40116	+86.663	0.058
2455439.37958	+86.510	0.056
2455704.56070	+86.620	0.065
2455776.46938	+86.611	0.064
2456005.71388	+86.564	0.134
2456033.63882	+86.633	0.058
2456078.51945	+86.566	0.061
2456488.39989	+86.763	0.044

Table A.16. HE 1523−1155

HJD	RV km s^{-1}	RV$_{err}$ km s^{-1}
2456756.69769	−48.312	0.034
2456796.67508	−46.377	0.051
2456888.38390	−40.622	0.040
2457110.72622	−46.063	0.069
2457142.65599	−44.028	0.037
2457168.61410	−42.363	0.026
2457225.44781	−39.130	0.042
2457239.39307	−38.552	0.020
2457258.36919	−38.016	0.042

Table A.17. HE 2201−0345

HJD	RV km s^{-1}	RV$_{err}$ km s^{-1}
2454314.59436	−54.804	0.053
2454338.51241	−54.763	0.098
2454373.44648	−54.627	0.078
2454665.70652	−53.021	0.093
2454964.70705	−50.946	0.142
2455009.67131	−50.441	0.093
2455059.48210	−50.167	0.071
2455126.49880	−49.927	0.067
2455344.66126	−51.510	0.053
2455415.47351	−52.802	0.062
2455439.41067	−53.130	0.051
2455503.33221	−54.321	0.155
2455531.36578	−54.418	0.185
2455704.66231	−56.625	0.042
2455776.49350	−57.152	0.086
2455882.30261	−58.114	0.092
2455898.30389	−58.260	0.091
2456033.73856	−58.053	0.236
2456078.70413	−58.791	0.096
2456139.62139	−58.890	0.102
2456518.50427	−59.730	0.532
2456530.61456	−59.760	0.062
2456603.44706	−59.703	0.121
2456886.51808	−59.808	0.085
2456956.46129	−60.095	0.197
2457192.70683	−60.170	0.059
2457257.54595	−60.008	0.100

Table A.18. HE 2312−0758

HJD	RV km s^{-1}	RV$_{err}$ km s^{-1}
2456191.43803	+38.553	0.050
2456213.45637	+38.391	0.054
2456488.71018	+34.121	0.045
2456518.67707	+33.749	0.051
2456528.66775	+33.640	0.063
2456545.61190	+33.228	0.046
2456887.52097	+30.174	0.067
2456917.53578	+30.435	0.073
2456956.48012	+30.255	0.074
2457225.62292	+30.102	0.062
2457257.56346	+30.139	0.048

Table A.19. HE 2330−0555

HJD	RV km s^{-1}	RV$_{err}$ km s^{-1}
2454314.711836	−234.968	0.046
2454373.550888	−235.089	0.052
2455059.605701	−235.218	0.054
2455080.608758	−235.039	0.108
2455126.539073	−235.182	0.059
2455176.414354	−235.118	0.142
2455415.633807	−235.179	0.052
2455439.497335	−235.104	0.060
2455478.573649	−235.114	0.078
2455531.439197	−235.126	0.094
2455776.707594	−235.231	0.070
2455796.607358	−235.370	0.091
2455882.421279	−235.048	0.045
2456141.696801	−234.927	0.092
2456241.363645	−234.912	0.212
2456530.642253	−235.139	0.066
2456887.546840	−235.386	0.094

Table A.20. HE 0039−2635

HJD	RV km s^{-1}	RV$_{err}$ km s^{-1}
2456241.41669	−52.078	0.023
2456518.71254	−43.400	0.023

Table A.21. HE 1031−0020

HJD	RV km s^{-1}	RV$_{err}$ km s^{-1}
2454219.42938	+69.718	0.103
2454254.44108	+69.319	0.152
2454406.74096	+69.519	0.119
2454459.64146	+69.839	0.141
2454464.63446	+69.944	0.086
2454481.61235	+69.524	0.145
2454516.55332	+69.634	0.096
2454793.76871	+69.565	0.136
2454909.51656	+69.473	0.124
2454930.53075	+69.308	0.067
2455174.70264	+69.198	0.095
2455207.60630	+69.142	0.075
2455544.74047	+68.903	0.114
2455620.49236	+68.592	0.096
2455915.79512	+68.460	0.222
2455944.58281	+67.917	0.197
2456033.38640	+68.077	0.098
2456241.74480	+67.609	0.138
2456399.40659	+67.486	0.120
2456722.48940	+66.819	0.149
2457110.39343	+66.361	0.227
2457142.44270	+66.111	0.106

Table A.22. LP 625−44

HJD	RV	RV_{err}
	km s^{-1}	km s^{-1}
2454219.72236	+38.955	0.039
2454254.65878	+38.870	0.111
2454285.56286	+39.027	0.060
2454314.49424	+38.911	0.041
2454338.41720	+38.770	0.047
2454373.35738	+38.773	0.051
2454625.62936	+38.051	0.038
2454665.57095	+38.081	0.093
2454930.74622	+37.306	0.046
2454964.69845	+37.168	0.059
2454987.52690	+37.153	0.036
2455059.43020	+36.853	0.075
2455344.60471	+36.007	0.060
2455415.37378	+35.652	0.057
2455439.39220	+35.608	0.057
2455620.75079	+34.869	0.059
2455704.58037	+34.615	0.062
2455776.41360	+34.301	0.048
2456005.74059	+33.446	0.086
2456033.68185	+33.154	0.106
2456062.71485	+33.086	0.091
2456078.55749	+32.913	0.069
2456488.41291	+30.863	0.052
2456574.33217	+30.479	0.037
2456579.32582	+30.406	0.081
2456756.74336	+29.588	0.167
2456796.71349	+29.225	0.068
2456887.37991	+28.872	0.056

Appendix B: Literature data for the single programme stars

Table B.1. Mean heliocentric radial velocities from the literature and total time-span covered for the single stars

Stellar ID	ΔT Total (days)	mean RV (this work) (km s^{-1})	mean RV (km s^{-1})	N	Ref
HE 0206−1916	4445	−199.509	−200.0	1	Aoki et al. (2007)
HE 1045+0226	1868	+131.498	+131.2	1	Cohen et al. (2013)
HE 2330−0555	4314	−235.124	−235.0	1	Aoki et al. (2007)
CS 30301−015	4352	+86.61	+85.5	1	Tsangarides et al. (2003)
			+86.5	1	Aoki et al. (2002c)
			+85.5	2	Lucatello et al. (2005)